IOP Conference Series: Materials Science and Engineering

PAPER • **OPEN ACCESS**

Influence of pack cementation time on the microstructure of Cu nanofoams processed by dealloying

To cite this article: Jenei Péter *et al* 2020 *IOP Conf. Ser.: Mater. Sci. Eng.* **903** 012047

IOP Conf. Series: Materials Science and Engineering **903** (2020) 012047 doi:10.1088/1757-899X/903/1/012047

Influence of pack cementation time on the microstructure of Cu nanofoams processed by dealloying

Péter Jenei[1*], Gigap Han[2], Pham Tran Hung[1], Heeman Choe[2] and Jenő Gubicza[1]

[1] Department of Materials Physics, Eötvös Loránd University, Budapest, Hungary
[2] School of Materials Science and Engineering, Kookmin University, Seoul, Republic of Korea

E-mail: jenei@metal.elte.hu

Abstract. Copper nanofoams were processed by dealloying for a prospective application as a Li-ion battery anode. The precursor material was produced by pack cementation. The effect of length of pack-cementation time on the pore structure and the microstructure of the struts was investigated in this study. It was found that for high pack-cementation times a hierarchical pore structure with nano- and micro-sized pores was formed. In addition, the longer the pack-cementation time, the lower the crystallite size and the dislocation density in the struts. A very high twin fault probability was also detected, irrespective of pack-cementation time.

1. Introduction

Metallic foams have a wide range of practical applications, such as energy absorbers in the automotive industry [1], non-flammable acoustic absorbers in vehicles and houses [2], filters [3], heat exchangers [4], implants in medicine [5], and anode materials in batteries [6]. The properties of these foams can be tailored with an appropriate design of pore structures [7]. Among metallic foams, nanofoams attract significant attention due to their extremely high specific surface area, since these materials have pore sizes <100 nm. The very high specific surface area can yield improved performances in some applications, such as for battery electrodes. Pore size and distribution can be designed by a careful selection of production method and processing conditions.

Various methods have been developed for the synthesis of nanofoams, such as the different dealloying processes (chemical, plasma, or metallic melt dealloying methods) [8-10]. During dealloying, the less noble metal in the alloy is dissolved by dealloying solutions, thereby creating pores in the final product. In many dealloying procedures, the precursor alloy is produced by powder metallurgy [8,11]. In this case, there is a high risk of crack formation during dealloying as a consequence of the incomplete sintering. Recently, a novel dealloying procedure has been developed in which the precursor material is processed without powder consolidation [6]. Namely, for manufacturing of the novel Cu nanofoams, first a precursor material was produced by pack-cementation technique, in which Al was coated onto a Cu foil that was subjected to annealing at a temperature between the melting points of Al and Cu. Then, Al diffused into Cu, forming Al and Cu intermetallic compounds. For long pack-cementation times, a pure Al phase also formed due to the high Al content of the material. Finally, Al atoms were removed from the sample by etching, and a Cu foam with fine pore structure was produced. If the precursor material contained both Al_2Cu and Al phases, a hierarchical pore structure with nano- and micro-sized pores was obtained [6]. The larger pores developed at the places of the former Al phase. The Cu foams

with hierarchical pore structures exhibited an improved electrochemical performance as anode in Li-ion batteries (e.g., showed a higher capacity compared to simple nanofoams [6]).

The pore size distribution and the microstructure of the foam struts strongly influence the functional properties of metallic foams. Therefore, it is very important to elucidate the effect of the processing conditions on the microstructure of nanofoams. In this paper, the influence of pack-cementation time on the microstructure of Cu nanofoams processed by dealloying is studied. The microstructure is characterized by scanning electron microscopy (SEM) and X-ray line profile analysis (XLPA). The latter method allows determination of the density of lattice defects (e.g., dislocations and twin faults) in the strut material.

2. Experimental materials and procedures

2.1. Sample preparation

In the present study, Cu nanofoams were processed using a dealloying technique. The precursor material was produced by pack cementation. First, a disk was cut from a Cu plate with a diameter of 11 mm and a thickness of 0.25 mm. Then, a blend of Al, Al_2O_3 and NH_4Cl powders were stacked on the Cu plate in a stainless steel container. In the pack-cementation step, the Cu plate in the powder bed was heat-treated at 800 ºC for different times: 3, 6, 12, and 15 h. During annealing, the Al particles were melted and Al atoms diffused into Cu, forming Al_2Cu phase [6]. For long pack-cementation times, an additional Al phase also formed. Al_2O_3 is a filler material in the powder blend, which slowed the process by decreasing the effective surface of the plate [6]. After pack cementation, the material was annealed in two stages, first at 700 ºC for 9 h and then at 500 ºC for 6 h, in order to homogenize the Al distribution in the Al_2Cu phase. It should be noted that the thickness of the samples increased with increasing pack-cementation time due to the incorporation of a higher amount of Al. For the 15 h time, the specimen thickness was enhanced from 0.25 mm to 1.1 mm [6]. In the dealloying process, in order to remove Al atoms from the material, the samples were chemically etched in water solution of HCl (using deionized water) at 45 ºC for 12 h. The pH of the HCl solution was set as 0.25. After dealloying, the etched disks were washed in ethanol and dried at 0.8 bar for a few hours. In the following, the samples are denoted according to the pack cementation time (3, 6, 12, and 15 h), however it should be emphasized that in this study the Cu nanofoams were studied after dealloying.

2.2. Methods for the characterization of the microstructure

The microstructure was investigated combining scanning SEM equipped with energy dispersive X-ray spectroscopy (EDS) and X-ray diffraction (XRD). The pore structure of the foam was studied by SEM using a FEI Quanta 3D electron microscope. The chemical composition of the foam struts were investigated by EDS, which was carried out with an electron energy of 20 keV. The phase composition of the foams was investigated by XRD using a Rigaku Smartlab X-ray diffractometer in Bragg–Brentano geometry with CuKα radiation (wavelength: 0.15418 nm). Moreover, XLPA was performed to examine the microstructure of the copper phase after dealloying. The X-ray line profiles were measured with a high-resolution rotating anode diffractometer (manufacturer: Rigaku, type: RA MultiMax-9) using $CuK\alpha_1$ radiation (wavelength: 0.15406 nm). The Debye–Scherrer diffraction rings were detected with two-dimensional imaging plates. The line profiles were determined by integrating the intensity along the rings, and the X-ray diffraction patterns were evaluated using the extended convolutional multiple whole profile (eCMWP) fitting method [12,13]. In this procedure, the diffraction pattern is fitted by the sum of a background spline and the convolution of the instrumental pattern and the theoretical line profiles related to the crystallite size, dislocations, and twin faults. Due to the very broad diffraction peaks, instrumental correction was not necessary. This evaluation method gives the area-weighted mean crystallite size ($\langle x \rangle_{area}$), the dislocation density, and the twin fault probability, where the twin fault probability in face-centered cubic (fcc) crystals is defined as the fraction of twin faults among the {111} lattice planes.

3. Results and discussion

3.1. Phase composition of the foams

Figure 1 shows the XRD patterns obtained on the Cu foams processed with different pack-cementation times. XRD analysis revealed the presence of Cu_2O and a very low amount of Al_2O_3 phase, beside the main fcc Cu phase, in the samples. The secondary phase content was characterized by the fraction of the integrated intensities of the peaks (i.e., the area under the peaks) related to the different phases in the XRD patterns after background subtraction. The fractions of the main and secondary phases are listed in Table 1. The Cu_2O phase was formed due to oxidation of the surface of the Cu foam struts. The fraction of this phase was 7–8% for the 3, 6 and 12 h pack-cementation times. For 15 h, the Cu_2O fraction increased to about 17%. The Al_2O_3 phase was a filler material in the pack-cementation process and a very small amount of this phase (≤ 1%) remained in the final dealloyed samples. In the main Cu phase, the remaining solute Al content was less than 2 at.%, as revealed by EDS, indicating that most of the aluminum was removed during the dealloying process.

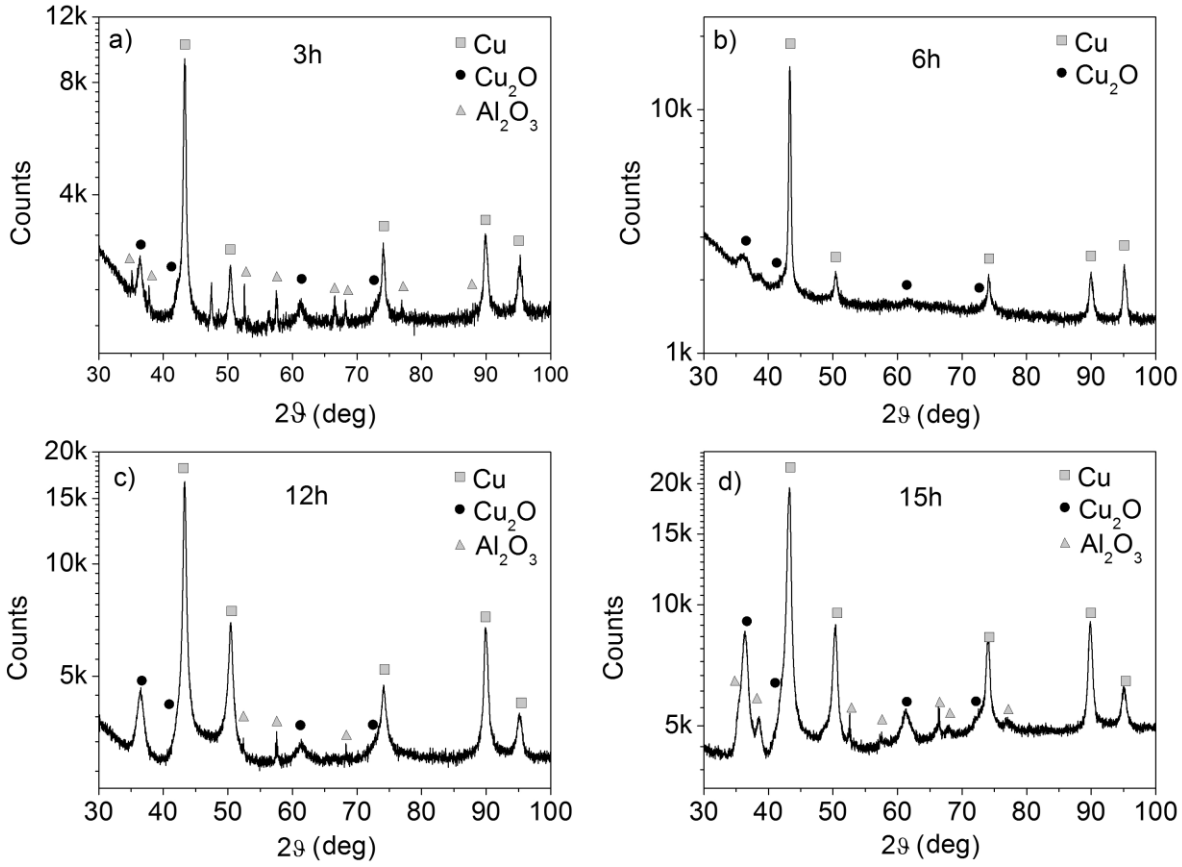

Figure 1. X-ray diffractograms for the Cu foam samples with pack cementation times of (a) 3 h, (b) 6 h, (c) 12 h, and (d) 15 h after dealloying.

Table 1. The chemical compositions of the bulk samples after pack-cementation but before dealloying, and the phase compositions of the dealloyed foams. The average ligament widths of the foams evaluated from SEM are also shown.

Pack-cementation time (h)	Composition of the samples after pack cementation (at.%)		Phase fractions in the nanofoams (%)			Ligament width (nm)
	Al (at.%)	Cu (at.%)	Cu	Cu_2O	Al_2O_3	
3	52.2 ± 0.6	47.8 ± 0.6	92 ± 3	7 ± 2	1 ± 1	200 ± 64
6	60.7 ± 3.1	39.3 ± 3.1	93 ± 2	7 ± 2	-	158 ± 26
12	75.0 ± 3.3	25.0 ± 3.3	92 ± 2	8 ± 2	<1	210 ± 101
15	79.6 ± 2.9	20.4 ± 2.9	83 ± 2	17 ± 2	<1	99 ± 47

3.2. Study of the pore structure by SEM

Figure 2 shows SEM images obtained for the lowest (3 h) and the highest (15 h) pack-cementation times. It can be seen that the morphologies of the pore structures in the two samples are very different. For low pack-cementation time (3 h), a homogenous nanoporous Cu foam was formed. Similar pore structure was observed for the sample processed by pack-cementation for 6 h. At the same time, for the long pack-cementation time (15 h), large micro-sized pores were also formed between the nanoporous struts of the foam. The same feature was found for the 12 h sample.

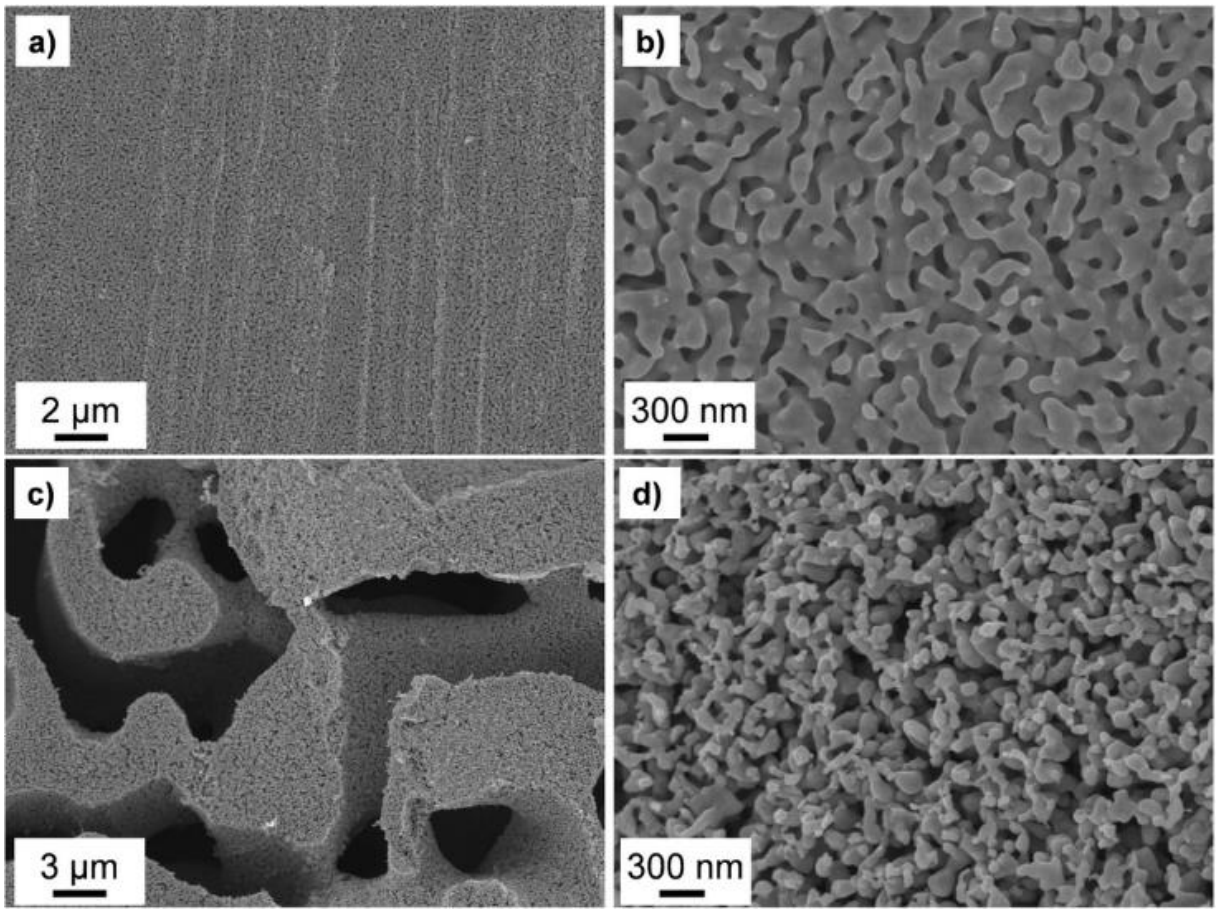

Figure 2. SEM images with different magnifications taken on the surfaces of the nanofoam samples processed with the pack-cementation times of (a-b) 3 h and (c-d) 15 h.

Difference in pore structures for short and long pack-cementation times is due to different amounts of Al diffused into Cu during pack-cementation. Table 1 shows the chemical composition of the bulk samples after pack cementation but before dealloying. It seems that the increase in pack-cementation time yielded a higher Al content. This can be easily understood if we consider that during pack cementation, Al atoms diffused from the molten Al into the solid Cu plate, and that, therefore, the longer pack-cementation time resulted in a higher Al concentration in the bulk samples before dealloying. For lower Al contents, only Al_2Cu intermetallic compound formed in the pack-cemented samples (specimens 3 h and 6 h). For high pack cementation times (12 and 15 h), when the Al:Cu ratio was higher than 2:1, a pure Al phase necessarily formed in the material. The dissolution of this pure Al phase caused the development of micropores after dealloying in the samples 12h and 15h, with mean micropore sizes of 5.5 ± 2.2 μm and 5.9 ± 2.4 μm, respectively. For all the four studied samples, the foam struts were built up from ligaments and the nanopores can be found between these ligaments. Therefore, the fineness of the nanopore structure in the struts can be characterized by the ligament sizes, which are listed in Table 1. The average ligament width was about 100–200 nm for the studied specimens.

3.3. Microstructure from XLPA

As an example, Figure 3 shows an eCMWP fitting of the XRD pattern for the sample 3h. The microstructural parameters obtained from XLPA are listed in Table 2. The crystallite size varied between 18 and 60 nm for the studied samples. These values are much smaller than the particle (ligament) sizes observed in the SEM images (see Table 1). This difference suggests that the ligaments consisted of smaller crystallites/grains. The Cu ligaments were formed during dealloying when Al atoms were dissolved from the Al_2Cu phase, and the remaining Cu atoms were clustered in an fcc Cu structure [14,15]. Table 2 shows that the Cu ligaments contained a significant amount of lattice defects, such as dislocations and twin faults. The order of magnitude of the dislocation density was 10^{14} m^{-2}, while the twin fault probability varied between 3.5 and 5.2%. It can be seen that the crystallite size and the dislocation density significantly decreased for high pack-cementation times (12 and 15 h). A less considerable change was observed for the twin fault probability.

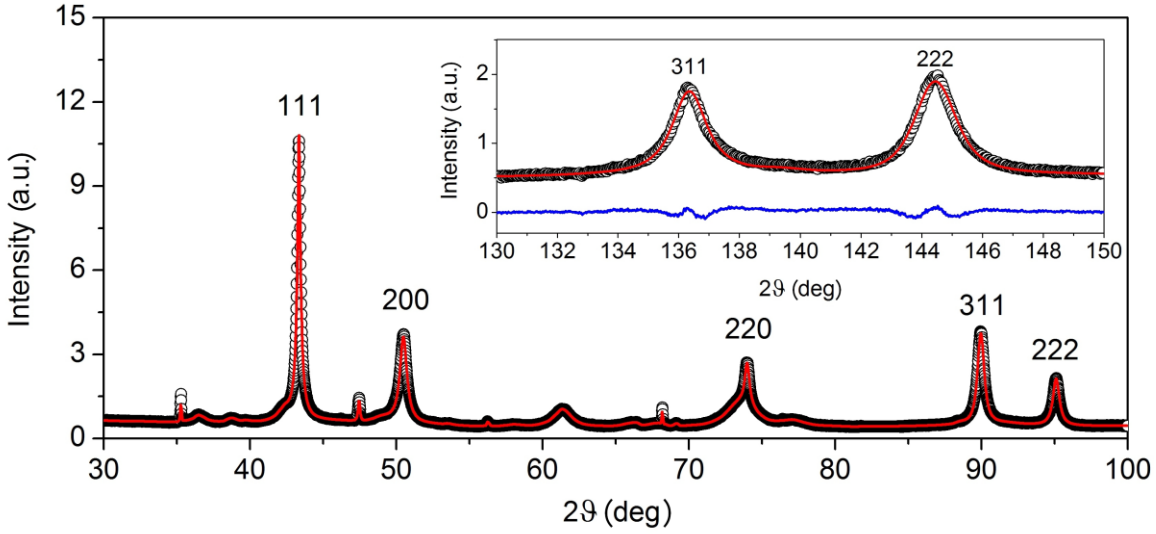

Figure 3. eCMWP fitting of the XRD pattern taken on the Cu foam processed with the 3 h pack-cementation time. The inset shows a magnified part of the diffractogram for a better visibility of the quality of fitting. The open circles and the red solid line represent the measured and the fitted XRD patterns, respectively. The blue curve in the inset shows the difference between the measured and fitted diffractograms.

Table 2. The area-weighted mean crystallite size ($\langle x \rangle_{area}$), the dislocation density (ρ), and the twin fault probability (β) for the Cu phase of the foams produced with different pack-cementation times.

Pack-cementation time (h)	$\langle x \rangle_{area}$ (nm)	ρ (10^{14} m^{-2})	β (%)
3	60 ± 6	8.6 ± 0.9	5.2 ± 0.5
6	60 ± 6	7 ± 0.7	3.5 ± 0.4
12	29 ± 4	2.6 ± 0.3	3.7 ± 0.4
15	18 ± 4	1.4 ± 0.3	3.6 ± 0.4

The dislocations and the twin faults observed in the Cu struts were grown-in defects formed during the nucleation of Cu ligaments in the dealloying step of sample processing. Dislocations can decrease the mismatch stresses between the neighboring Cu grains in the struts. For long pack-cementation times, the samples contained many Cu grains located on the surfaces of the struts at the large micro-sized pores, and these grains had lower numbers of neighbors. Therefore, these materials have lower dislocation densities.

During the dealloying process, when a new Cu grain nucleates on a pre-existing ligament non-epitaxially, the new grain is preferably separated from the older one by twin fault as this has the lowest energy among the grain boundaries in fcc crystals. Therefore, a very high twin fault probability was detected in the present Cu nanofoams, almost irrespective of the pack-cementation time. It should be noted that further research is planned to study the influence of the pore structure and the lattice defects on the mechanical behavior of the samples manufactured with different pack-cementation times.

4. Summary

The present study shows the influence of pack-cementation time on the microstructure of Cu nanofoams processed by dealloying. To the authors' best knowledge, this is the first investigation in the literature, which quantifies the lattice defect density in the struts of foams obtained by dealloying. The following conclusions were drawn:

1) The pore structure can be tuned with an appropriate selection of pack-cementation time. The higher pack-cementation time induced hierarchically structured materials due to the larger Al content. The ligament width was about 100–200 nm, while the size of the large pores was about 5–6 μm.
2) A significant amount of lattice defects (dislocations and twin faults) was detected in the main Cu phase of the foams, irrespectively of the pack-cementation time. It was found that the dislocation density and the crystallite size decreased considerably with increasing pack-cementation time. The twin fault probability in the Cu phase was very high (3.5–5.2%) for all studied samples, as these boundaries have low energy and, therefore, were preferably formed during growing of the ligaments for the accommodation of misorientations inside the struts.

Acknowledgements

This research was supported by the Hungarian-Korean bilateral Research program (TÉT) No. 2018-2.1.17-TÉT-KR-2018-00003**.** This work was financed partly by the Ministry of Human Capacities of Hungary within the ELTE University Excellence program (1783-3/2018/FEKUTSRAT). H. Choe also acknowledges support from the International Research & Development Program of the National Research Foundation of Korea (2018K1A3A1A39086825). P. Jenei acknowledges the financial support of János Bolyai Research Scholarship of the Hungarian Academy of Sciences and ÚNKP-19-4 New National Excellence Program of the Ministry for Innovation and Technology.

References

[1] Kretz R, Hausberger K, Götzinger B 2002 *Adv. Eng. Mater*. **4** 781–85
[2] Miyoshi T, Itoh M, Akiyama S, Kitahara A 2000 *Adv. Eng. Mater*. **2** 179–183
[3] Kim S, Lee C W 2014 *Proc. Mater. Sci.* **4** 305–309
[4] Evans A G, Hutchinson J W, Ashby M F 1998 *Prog. Mater. Sci.* **43** 171–221
[5] Choi H, Shilko S, Gubicza J, Choe H 2017 *J. Mech Behav Biomed Mater* **72** 66–73
[6] Han G, Um J H, Park H, Hong K, Yoon W S, Choe H 2019 *Scripta Materialia* **163** 9–13
[7] F García-Moreno 2016 *Materials* **9** 85–27
[8] Jo H, Cho Y H, Choi M, Cho J, Um J H, Sung Y E, Choe H 2014 *Mater. Chem. Phys.* **145** 6–11
[9] Wada T, Yubuta K, Inoue A, Kato H 2011 *Mater. Lett.* **65** 1076–78
[10] Lee G H, An S, Jang S W, Hwang S, Lim S H, Han S 2017 *Thin Solid Films* **631** 147–51
[11] Chen F, Chen X, Zou L, Yao Y, Lin Y, Shen Q, Lavernia E J, Zhang L 2016 *Mater. Sci. Eng. A* **660** 241–250
[12] Ribárik G, Gubicza J, Ungár T 2004 *Mater. Sci. Eng. A* **387–389** 343–347
[13] Balogh L, Ribárik G, Ungár T 2006 *J. Appl. Phys.* **100** 023512
[14] Liu W, Zhang S, Li N, Zheng J, An S, Li G 2012 *Int. J. Electrochem. Sci.* **7** 7993–8006
[15] Erlebacher J, Aziz M J, Karma A, Dimitrov N, Sieradzki K 2001 *Nature* **410** 450–453